TU Delft

Delft University of Technology

Provision of Ramp-rate Limitation as Ancillary Service from Distribution to Transmission System

Definitions and Methodologies for Control and Sizing of Central Battery Energy Storage System

Gkavanoudis, Spyros I.; Malamaki, Kyriaki Nefeli D.; Kontis, Eleftherios O.; Demoulias, Charis S.; Shekhar, Aditya; Mushtaq, Umer; Venu, Sagar Bandi

DOI
10.35833/MPCE.2022.000595

Publication date
2023

Document Version
Final published version

Published in
Journal of Modern Power Systems and Clean Energy

Citation (APA)
Gkavanoudis, S. I., Malamaki, K. N. D., Kontis, E. O., Demoulias, C. S., Shekhar, A., Mushtaq, U., & Venu, S. B. (2023). Provision of Ramp-rate Limitation as Ancillary Service from Distribution to Transmission System: Definitions and Methodologies for Control and Sizing of Central Battery Energy Storage System. *Journal of Modern Power Systems and Clean Energy*, *11*(5), 1507-1518. https://doi.org/10.35833/MPCE.2022.000595

Important note
To cite this publication, please use the final published version (if applicable).
Please check the document version above.

Copyright
Other than for strictly personal use, it is not permitted to download, forward or distribute the text or part of it, without the consent of the author(s) and/or copyright holder(s), unless the work is under an open content license such as Creative Commons.

Takedown policy
Please contact us and provide details if you believe this document breaches copyrights.
We will remove access to the work immediately and investigate your claim.

This work is downloaded from Delft University of Technology.
For technical reasons the number of authors shown on this cover page is limited to a maximum of 10.

Green Open Access added to TU Delft Institutional Repository

'You share, we take care!' - Taverne project

https://www.openaccess.nl/en/you-share-we-take-care

Otherwise as indicated in the copyright section: the publisher is the copyright holder of this work and the author uses the Dutch legislation to make this work public.

Provision of Ramp-rate Limitation as Ancillary Service from Distribution to Transmission System: Definitions and Methodologies for Control and Sizing of Central Battery Energy Storage System

Spyros I. Gkavanoudis, Kyriaki-Nefeli D. Malamaki, Eleftherios O. Kontis, Aditya Shekhar, Umer Mushtaq, Sagar Bandi Venu, and Charis S. Demoulias

***Abstract*—The variability of the output power of distributed renewable energy sources (DRESs) that originate from the fast-changing climatic conditions can negatively affect the grid stability. Therefore, grid operators have incorporated ramp-rate limitations (RRLs) for the injected DRES power in the grid codes. As the DRES penetration levels increase, the mitigation of high-power ramps is no longer considered as a system support function but rather an ancillary service (AS). Energy storage systems (ESSs) coordinated by RR control algorithms are often applied to mitigate these power fluctuations. However, no unified definition of active power ramps, which is essential to treat the RRL as AS, currently exists. This paper assesses the various definitions for ramp-rate RR and proposes RRL method control for a central battery ESS (BESS) in distribution systems (DSs). The ultimate objective is to restrain high-power ramps at the distribution transformer level so that RRL can be traded as AS to the upstream transmission system (TS). The proposed control is based on the direct control of the $\Delta P/\Delta t$, which means that the control parameters are directly correlated with the RR requirements included in the grid codes. In addition, a novel method for restoring the state of charge (SoC) within a specific range following a high ramp-up/down event is proposed. Finally, a parametric method for estimating the sizing of central BESSs (BESS sizing for short) is developed. The BESS sizing is determined by considering the RR requirements, the DRES units, and the load mix of the examined DS. The BESS sizing is directly related to the constant RR achieved using the proposed control. Finally, the proposed methodologies are validated through simulations in MATLAB/Simulink and laboratory tests in a commercially available BESS.**

***Index Terms*—Battery energy storage system, distributed renewable energy resource, sizing, distribution system, transmission system, ramp-rate limitation, state of charge.**

NOMENCLATURE

ΔE_{SoC}	Energy absorbed-released for state of charge (SoC) restoration
ΔE_{RR}	Energy absorbed-released for ramp-rate (RR) limitation (RRL)
ΔP	Actual power variation
$\Delta P_{\max}$	The maximum power variation for defining a high-power ramp event
ΔP_{SoC}	Charging-discharging power for SoC restoration
ΔP_{m1}, ΔP_{m2}, ΔP_{m3}	Power variations computed with definitions 1, 2, and 3
$\Delta P/\Delta t$	Rate of change of active power
ΔSoC	SoC dead-band
Δt	Time window for RR computation
Δt_{SoC}	The maximum SoC restoration time
τ	Duration of rolling window (averaging time)
E^p_{BESS}	Battery energy storage system (BESS) energy absorbed
E^n_{BESS}	BESS energy released
E_{BESS}	BESS capacity
k_{DRES}	Distributed renewable energy source (DRES) power variation coefficient
$k_{DRES,PV}$	Photovoltaic (PV) power variation coefficient
$k_{DRES,WTG}$	Wind turbine generator (WTG) power variation coefficient
$k_{LD,dom}$	Domestic load power variation coefficient

Manuscript received: September 14, 2022; revised: January 8, 2023; accepted: February 27, 2023. Date of CrossCheck: February 27, 2023. Date of online publication: April 5, 2023.

This work was part of and supported by the European Union, Horizon 2020 project "EASY-RES" with G. A.: 764090.

This article is distributed under the terms of the Creative Commons Attribution 4.0 International License (http://creativecommons.org/licenses/by/4.0/).

S. I. Gkavanoudis, K.-N. D. Malamaki (corresponding author), E. O. Kontis, and C. S. Demoulias are with the Department of Electrical & Computer Engineering, Aristotle University of Thessaloniki, Thessaloniki, Greece (e-mail: s.gkavan@gmail.com; kyriaki_nefeli@hotmail.com; ekontis@auth.gr; chdimoul@auth.gr).

A. Shekhar and U. Mushtaq are with the Electrical Engineering, Mathematics & Computer Science Department, Delft University of Technology, Delft, Netherlands (e-mail: a.shekhar@tudelft.nl; u.mushtaq@tudelft.nl).

S. B. Venu is with FENECON Gmbh, Deggendorf, Germany (e-mail: sagar.venu@fenecon.de).

DOI: 10.35833/MPCE.2022.000595

$k_{LD,ind}$	Industrial load power variation coefficient
k_{LD}	Load power variation coefficient
k_p	DRES penetration level coefficient
L_1, L_2	Upper and lower bounds for ramp event
p	Instantaneous active power
P_{BESS}	BESS power
P_{in}	Active power measurement at point of interconnection (POI)
P_{out}	Smoothed reference power
P_{smooth}	Smoothed active power
P_{ref}, Q_{ref}	Active and reactive reference power
RR_L	RRL
RR_L^N	The maximum negative RRL
RR_L^P	The maximum positive RRL
RR_M	The maximum RR measured at POI
$RR_{M,dom}$	The maximum RR of domestic load
$RR_{M,ind}$	The maximum RR of industrial load
$RR_{M,PV}$	The maximum RR of PV
$RR_{M,WTG}$	The maximum RR of WTG
S_{tr}	Rated power of distribution transformer
S_{DRES}	DRES power
T_r	Threshold for ramp event identification
u_1	Portion of PV load in DRES mixture
u_2	Portion of WTG load in DRES mixture, $u_2 = 1 - u_1$
w_1	Portion of domestic load in load mixture
w_2	Portion of industrial load in load mixture, $w_2 = 1 - w_1$

I. Introduction

PHOTOVOLTAICS (PVs) and wind turbines are currently the two most popular distributed renewable energy sources (DRESs). Nevertheless, despite their highly beneficial nature and the ever-decreasing installation costs, their penetration into modern power systems causes a series of technical issues that are mainly related to the intermittent and volatile nature [1]. In cases of high DRES penetration levels, the volatility of the injected power can potentially lead to significant voltage and frequency deviations [2], [3], which pose challenges to grid stability [4]. To mitigate the effects of active power fluctuations on power quality and grid stability, transmission system operators (TSOs) deploy grid codes that impose specific ramp-rate (RR) limitations (RRLs) on DRESs that are directly connected to the transmission system (TS) [5], [6].

Concerning this issue, the European Union Commission regulation 2016/631 [7] states that the relevant system operator shall specify, in coordination with the relevant TSO, the minimum and maximum limits on rates of change of active power output (ramping limits) in both up and down directions of change of active power output for a power-generating module, taking into consideration the specific characteristics of prime mover technology. In this context, the European Network of TSO for Electricity (ENTSO-E) has provided details in [8] regarding the upward RRL of generators following accidental disconnection from the power grid. As stated in [8], in Baltic and Nordic countries and in most Central European countries, this value is limited to 10%/min, i.e., 10% of the nameplate capacity per minute. Nevertheless, several national codes impose different limits. For instance, in France and Ireland, RRLs are set to be 4 MW/min and 30 MW/min [9], respectively, while in Denmark, RRL is set by Energinet at between 1% and 20% of the maximum capacity and is always below 60 MW/min [9]. In Scotland, England, and Wales, RRs are limited by the size of the generation units [10], [11].

Additionally, it is worth noting that different RRL requirements are applied globally. For instance, the Australian Market Operator requests at least a 3%/min RRL [11], whereas according to the Hawaii Electric Company, RRLs should be limited to 1 MW every 2 s or 2 MW/min [11]. The Puerto Rico Electric Power Authority requests a 10%/min RRL [12]. In China and India, the RRL requirements are imposed based on the nominal power of the unit [10], [11]. However, every national TSO imposes different limits. For instance, the State Grid Corporation of China requests large wind farms (WFs) with capacities higher than 150 MW to limit their RRLs to 100 MW every 10 min on average and to 30 MW every 1 min on average, whereas for WFs with capacities lower than 30 MW, RRLs are set to be 2 MW every 10 min on average and 6 MW every 1 min on average [10].

Clearly, many different RRL requirements are applied globally. Another noteworthy fact is that although high-power ramps can be easily identified visually, in existing grid codes, no unified definition of active power ramps exists [5], [6]. Most grid codes express this requirement as a per-minute limitation but do not define how the power ramps are measured, e.g., minute-to-minute average power [13]. Another important issue is that existing standards and grid codes focus only on large-scale DRESs and do not provide specifications for small-scale DRESs connected to distribution systems (DSs) [14].

However, due to the ever-increasing DRES penetration, several small-scale DRESs are connected to DSs, which considerably affects overall grid stability [15]. As a promising solution to compensating for the adverse effects of small-scale DRESs on grid dynamics, central battery energy storage systems (BESSs) are placed at the point of interconnection (POI) with TS. A significant advantage of this method is that DS operators can use these BESSs to provide RRL as ancillary service (AS) from DSs to the upstream TS. In this case, in order to meet the RRL requirements imposed by grid codes, the BESS should be properly controlled and sized.

Several methods have been used to smooth output power fluctuations of DRESs. These methods can be classified into three categories: ① moving average (MA) based methods [16], [17]; ② low-pass filter (LPF) based methods [18], [19]; and ③ direct RR control based methods [20], [21]. MA and LPF based methods are the most widely adopted

since they are easy to implement and have low computational burden. However, these methods also present some important disadvantages [22] such as the occurrence of both a "memory effect" and over-smoothing, which may lead to increased BESS capacity and reduced battery lifetime. In addition, no correlation can be defined between the control parameters of these methods and the obtained RRL. Therefore, MA and LPF based methods cannot be used to provide RRL as AS. However, direct RR control based methods can guarantee a specific RRL, leading to reduced BESS sizing as compared with MA and LPF based methods [22], [23]. However, existing direct RRL methods do not consider the state of charge (SoC) of the BESS prior to the initiation of the smoothing function [22]. Therefore, the BESS may reach its SoC limits unexpectedly, causing unforeseen ramps [22].

Concerning optimal energy storage system (ESS) sizing for RRL, many research works are reported in the literature. Several studies propose ESS sizing methods based on the specific characteristics of DRES technology. For instance, in [24]-[26], optimal storage sizing for RRL in WFs is investigated, while in [27] and [28], sizing methodologies for RRL of PV parks are presented. However, the aforementioned methodologies are technology-specific, thus they cannot be applied for the sizing of central BESSs (BESS sizing for short) in DSs that host several types of loads and DRESs. To meet this requirement, deterministic and probabilistic methods have been developed [29]. Deterministic methods are based on analyzing several power profiles, ideally obtained at POI with TS to define the ESS capacity that optimally fits the user-defined performance criteria. Nevertheless, the implementation of these methods is intricate and computationally intensive, due to the high granularity of the required data [30]. Therefore, probabilistic methods have been proposed as alternatives. These methods are based on historical climate and consumption data. Through statistical [31] or clustering analysis [30], these data are then used to determine representative power profiles for use in optimal storage sizing. However, these methods require a vast amount of historical data to achieve satisfactory performance.

The scope of this paper is to develop a holistic method for provisioning of RRL as AS from DSs to the upstream TS. To achieve this objective, the following tasks are performed. The various definitions used to calculate active power ramps are first assessed. A method for controlling the BESSs installed at POI with TS is then developed, which aims to restrain the power ramps toward TS. The proposed control method is complemented by restoring the SoC. Finally, a novel parametric method for BESS sizing is proposed. The contributions of this paper can be summarized as follows.

1) The available definitions for computing active power ramps are compared, and the most suitable definition for RES applications is proposed.

2) A control method for central BESSs aiming at restraining high-power ramps toward TS is proposed. A unique advantage of the proposed control method is that it does not require averaging functions or filters. The proposed control method in fact restrains RRs by directly calculating and controlling the RR $\Delta P/\Delta t$ (imposed by the adopted grid code definition/requirement), thus ensuring that actual ramps will never exceed the maximum permissible limits.

3) A method for restoring SoC is developed. The novelty of this method is that the maximum SoC restoration time can be defined parametrically while always respecting the RRL of output power. Therefore, the method can be altered to satisfy the unique requirements of each storage technology. It also has a low computational burden since it is based on simple arithmetic operations without any control loops.

4) A novel parametric method for BESS sizing is proposed. The distinct advantage of the developed method is that the required BESS sizing for RRL is determined without the need for long-term measurements at POI. Accordingly, the proposed method is based solely on the power variation characteristics of the individual loads and DRESs connected to the examined DS. The proposed method receives the size of the interconnection transformer, the types and sizes of the DRESs and loads that are connected to the DS, and the maximum $\Delta P/\Delta t$ imposed by the TSO. Using these inputs and the representative generation and consumption profiles, the proposed method quickly computes the required BESS for RRL.

It is worth noting that the proposed methods for SoC restoration and BESS sizing present high novelty, as no similar methods have been reported so far. Finally, because the proposed methods for BESS control, SoC restoration, and sizing is built around the definition of RR, a complete framework that facilitates the provision of RRL as AS from DSs to the upstream TS is provided.

The remainder of this paper is structured as follows. Section II presents the definitions of RRL. Section III presents the control of central BESS for RRL, and Section IV describes the BESS control method for SoC restoration. Section V presents the proposed method for BESS sizing. Section VI describes the validation of the proposed method through simulations and laboratory tests. Finally, Section VII summarizes the major contributions and concludes the paper.

II. Definitions of RRL

Although it is easy to visually identify ramps, there is no consensus on the accepted formal mathematical definition of a ramp event. Each paper or report uses a different computational method depending on the scope of the study. In [13], the characteristics for identifying ramp events are outlined. To define a ramp, three key characteristics should be determined: direction, duration, and magnitude. Regarding the direction, there are two basic types of ramps: upward (also known as ramp-ups) and downward (ramp-downs). However, since the values of ramp magnitude range from positive to negative, a ramp can be characterized using only its magnitude and duration features. The sign of the magnitude indicates the ramp direction, where values of positive or negative magnitude correspond to upward or downward ramps, respectively. Regarding the magnitude and duration, a comparison of current and previous values of the power is required to measure a ramp. Then, it is necessary to establish a threshold to indicate whether that difference is considered

in a ramp event or not.

One difficulty arises from the definition of the current and past instants. The time interval is crucial to define the ramp. Choosing a setting value depends on the type of ramp that must be detected. Another difficulty is that when using some definitions, only two discrete points are compared, which in turn neglects the power behavior inside the period between those points in time. In [13], there are two useful definitions cited in other reports.

1) Definition 1 (Def. 1): a ramp event is considered to occur at the start of an interval if the magnitude of the increase or decrease in the power measured at time Δt ahead of the interval is greater than a predefined threshold T_r:

$$p(t+\Delta t)-p(t)>T_r \tag{1}$$

2) Definition 2 (Def. 2): a ramp event considers the minimum and maximum values of the measurements between the two endpoints (inclusive):

$$\max[p(t,t+\Delta t)]>T_r \tag{2}$$

Def. 2 avoids the issue of neglecting whatever occurs within the period between the present moment and the past moment. However, this results in the detection of ramps for longer periods. Besides, both definitions make it impossible to filter ramps caused by fast events. This can be observed in Fig. 1, where the ramps detected using both definitions are compared. Sudden increases and decreases in power are analyzed. All power changes take place in less than 1 min. Figure 1(a) shows that both definitions detect the power increase at t_0. Figure 1(b) and (c) shows that after 20 s and 40 s, the ramp detected by Def. 2 is still high, although the event has dimmed.

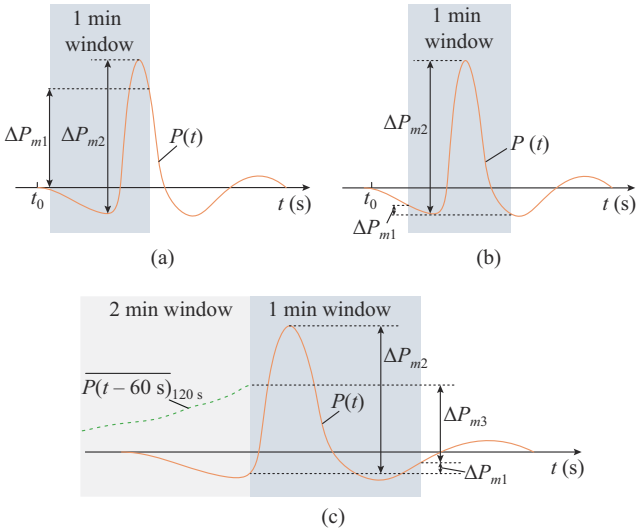

Fig. 1. Power variation computation for a 1 min window according to three definitions. (a) $\Delta P_{m1}(t=t_0)$. (b) $\Delta P_{m2}(t=t_0+20\text{ s})$. (c) $\Delta P_{m3}(t=t_0+40\text{ s})$.

3) Definition 3 (Def. 3): another definition that avoids these issues is described in [32]. In addition to the duration of the period under evaluation being established, an averaging time τ for power measurements must be used [32]. Under this assumption, the ramp event occurs when the current measurement is outside the range defined by $L_1(t_o)$ and $L_2(t_o)$:

$$L_1(t_o)=\overline{P(t_o+\Delta t)}_\tau-\left|\Delta P_{\max}\right| \tag{3}$$

$$L_2(t_o)=\overline{P(t_o+\Delta t)}_\tau+\left|\Delta P_{\max}\right| \tag{4}$$

A ramp event occurs if one of two following conditions are fulfilled:

$$P(t_o)<\overline{P(t_o+\Delta t)}_\tau-\left|\Delta P_{\max}\right| \tag{5}$$

$$P(t_o)>\overline{P(t_o+\Delta t)}_\tau+\left|\Delta P_{\max}\right| \tag{6}$$

Hence, it is obvious that the power variation is:

$$\Delta P=P(t_o)-\overline{P(t_o+\Delta t)}_\tau \tag{7}$$

A ramp is identified when $\Delta P>|\Delta P_{\max}|$ or $\Delta P<-|\Delta P_{\max}|$. Figure 1(c) shows the effect of computing the power variation using the mean value in a rolling window as the past value. In this case, the variation detected is higher than that detected by Def. 1 but is less than that detected by Def. 2. Def. 3 allows the operator to discriminate the timeframe of the ramps to be detected, filtering out the low- and high-frequency events. The parameters Δt and τ must be appropriately selected to detect the ramps under study.

These three definitions are compared when applied to the variations in the PV power profiles shown in Fig. 2(a). Figure 2(b) shows the computed RR when the three definitions are applied to the power profile shown in Fig. 2(a). The red horizontal line in Fig. 2 corresponds to the maximum permissible RRL, e.g., 100 W/min, corresponding to 10%/min for an installation of 1 kW.

Def. 2 clearly produces the highest variations. Def. 1, which compares two instant values separated by 60 s, produces slightly lower results. Def. 3 compares the current measurement with the average over the past 120 s, resulting in notably smaller power variations. The plot on the right in Fig. 2(b) shows the evolution of the active power variations, i.e., RR for 4 min. It can be also seen that the total duration for which the RR is computed by Def. 2 exceeds the maximum permissible RR, i.e., an active ramp-up or ramp-down event is higher in comparison with that in the other two cases. Finally, in Table I, the numbers of periods (measured in *s*) in which a ramp event is active using each definition are compared. These results are in accordance with those shown in Figs. 1 and 2.

TABLE I
NUMBER OF PERIODS WITH ACTIVE RAMPS FOR EACH DEFINITION

Definition	Number of periods with active ramp	Percentage of time (%)
Def. 1	7722	21.2
Def. 2	12714	34.9
Def. 3	6294	17.3

In this paper, Def. 3 is proposed as the most suitable for calculating ramp-ups and ramp-downs. Using the mean value in a rolling window as the past value produces a more robust RR calculation that is less affected by the instantaneous value of the power at the start of the interval. Nevertheless, for the remainder of the papers, Def. 1 is used for the following reasons: ① most of the existing grid codes adopt

Def. 1 to compute the RR since calculating only the power difference between the two instants is more straight-forward; ② Def. 1 is more sensitive in detecting high-power ramps; ③ if the length of the rolling window is close to zero, Def. 3 is equivalent to Def. 1. Thus, if RRL is achieved using Def. 1, it is ensured that RRL is also attained by Def. 3. Def. 2 is not considered as a suitable choice since it does not provide any means of filtering ramps caused by fast events.

III. Control of Central BESS for RRL

To comply with the TSO-imposed RRL, the integration of a central BESS is proposed, which is located near the DS transformer (DST) so as to provide RRL as AS to the upstream TS. RRL is provided as long as the measured RR at POI is less than the maximum permissible value. In this sense, the BESS control should generate a power profile for specific selectable RR. We propose a more suitable method for directly controlling RR of DRES output power. This is critical because all grid codes on RRL are expressed by $\Delta P/\Delta t$. At this point, we should note that the use of the maximum RR as a parameter in the BESS controller ensures that the proposed method is directly applicable to all requirements irrespective of the RR definition used. The clear advantage of the proposed method over others that use an LPF or MA function is that, in the latter cases, no clear relationship exists between the cutoff frequency of the LPF or the time interval of the averaging function with the required RRL. In addition, by properly selecting Δt, it is possible to absorb any high-power variations, which appear between the start and end points of the analysis window.

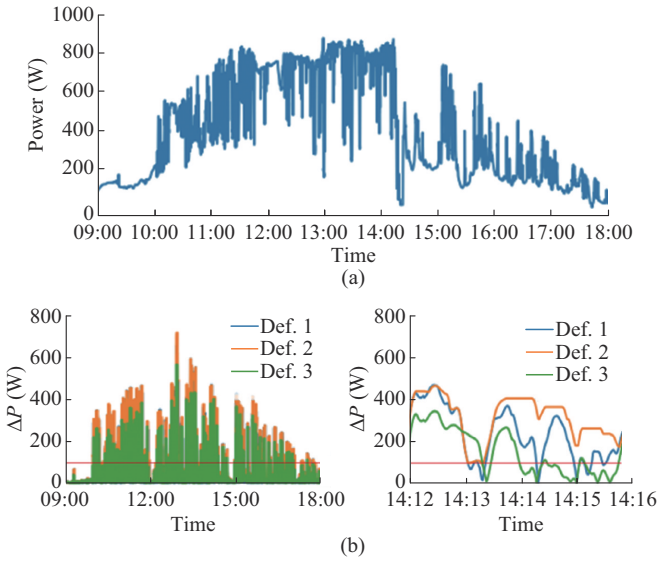

Fig. 2. Comparison of RR definitions. (a) Variations in PV power profile. (b) Power variations measured using each definition.

The topology and the overall control scheme of BESS RR are depicted in Fig. 3. The grid voltage and line currents are fed to the BESS controller for the measurement of the active power. The sampling rate of the measurements should not exceed Δt. The main control block for producing the smoothed active power profile (of specific RR) is shown in Fig. 4. This block takes as input the fluctuating P_{in} and RR_L^p and RR_L^n, while considering both ramp-ups and ramp-downs. ΔP_{SoC} is a parameter that modifies P_{in} and is used for the SoC restoration, as described in the following section.

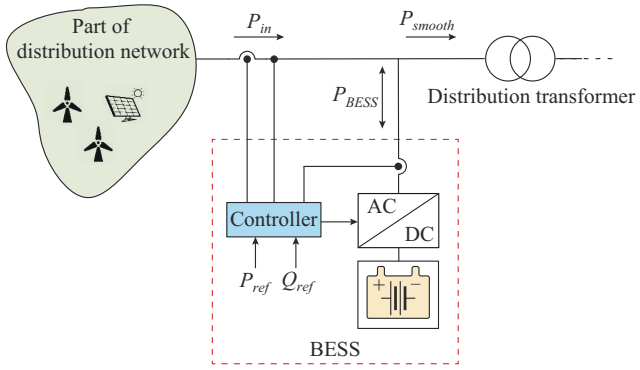

Fig. 3. Topology and overall control scheme of BESS RR.

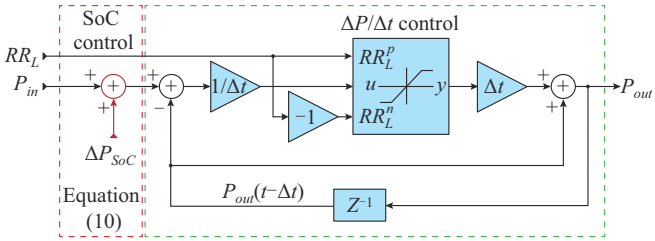

Fig. 4. Main control block for producing smoothed active power profile.

IV. BESS Control Method for SoC Restoration

An effective ESS should be complemented by SoC restoration control. The aim of this control is to restore the SoC to a predefined range, so that the BESS is always capable of smoothing ramp-ups and ramp-downs. This paper proposes a novel SoC restoration control method, which aims to restore SoC to 50% without violating the maximum RRL. To achieve this, the proposed SoC restoration control method modifies P_{in} by adding/subtracting ΔP_{SoC}, as shown in Fig. 4. A major aspect of this control method is that the SoC restoration signal ΔP_{SoC} is added prior to the RR control. This ensures that RRL of the output power will not be violated. ΔP_{SoC} is pre-calculated in an analytical form based on Δt_{SoC} and E_{BESS}. Moreover, ΔP_{SoC} is inserted directly as an input to the proposed control method. The maximum restoration time corresponds to the time needed for a fully charged BESS to restore its SoC to 50%. In addition, an important feature of the proposed control method is that it does not employ any controller so as to reach the SoC reference value but only a dead-band. Accordingly, the SoC restoration control is deactivated in order to prevent the SoC from oscillating around the reference value. The proposed control and the value of the dead-band are illustrated in Fig. 5. In the following analysis, the proposed control method considers the worst-case scenario, i.e., an abrupt step change in the active power exchange at the POI. Therefore, the restoration time inserted as a parameter in the control method is referred to as the maximum time. In this case, during BESS charging/discharging, ΔP_{SoC} uses the maximum permissible value, thereby exploit-

ing the entire RR margin. This causes the total power to take on a trapezoidal form with the slope angle of the non-parallel sides defined by the RRL. According to Fig. 5, it is assumed that the power absorbed for limiting the RR is equal to ΔE_{RR}. To restore SoC, BESS has to release the same amount of energy ($\Delta E_{RR}=\Delta E_{SoC}$). Based on the above assertions, the trapezoidal energy recovery of Fig. 5 is derived and can be analytically formulated.

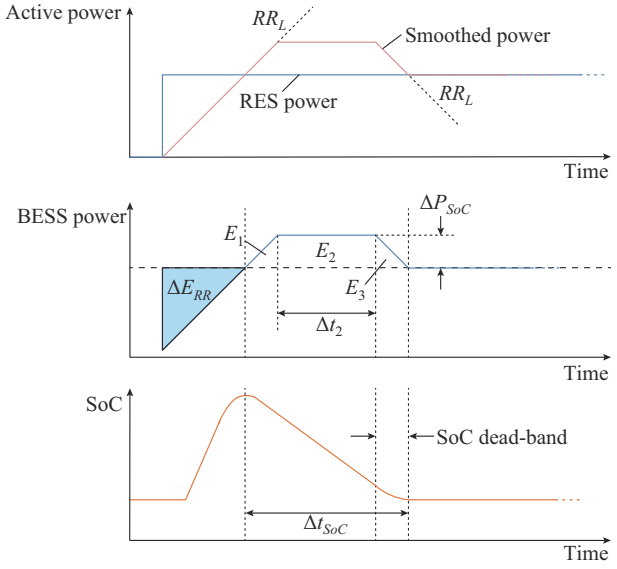

Fig. 5. Proposed control and value of dead-band.

ΔP_{SoC} can be calculated as:

$$\Delta E_{SoC}=E_1+E_2+E_3 \tag{8}$$

$$\Delta E_{SoC}=\frac{\Delta P_{SoC}^2}{RR_L}+\Delta P_{SoC}\Delta t_2 \tag{9}$$

$$\Delta P_{SoC}=\frac{-\Delta t_{SoC}+\sqrt{\Delta t_{SoC}^2-\dfrac{4}{RR_L}\Delta E_{SoC}}}{2}RR_L \tag{10}$$

ΔE_{SoC} is set equal to half the total BESS capacity. Following the deactivation of the SoC control, the BESS power will not instantly become zero, but will continue decreasing with the same RR until it becomes zero. The time interval between the deactivation of the SoC control and the moment at which the P_{BESS} becomes zero determines the dead-band ΔSoC:

$$\Delta E_{SoC}=\frac{1}{2}\Delta t_{SoC}\Delta P_{SoC}=\frac{1}{2}\frac{\Delta P_{SoC}^2}{RR_L} \tag{11}$$

$$\Delta SoC=\frac{\Delta E_{SoC}}{E_{BESS}} \tag{12}$$

Thus, the recovery control is deactivated at the SoC level of $50\pm\Delta SoC$. Without this dead-band, SoC oscillates infinitely around the reference SoC. The novelty of the proposed control method is that: ① it is embedded in the RR control method, and therefore, the maximum RR is always respected; ② the maximum SoC restoration time is calculated based on the BESS energy and desired RR and then inserted into the control method; in this way, it can be predetermined; and ③ the computation burden is really low since it is based on simple arithmetic operations.

V. BESS Sizing for RRL

The proposed BESS sizing method considers a DS consisting of both DRES units and loads. This provides a fast way to estimate the required size without the need for long-term measurements at POI, which is based on the power variation characteristics of individual loads or DRESs. Therefore, a set of parameters, e.g., S_{tr}, k_p, RR_L, k_{LD}, k_{DRES}, and RR_M, is identified that affects the BESS sizing.

S_{tr}, k_p, and RR_L can be easily identified, since they are known parameters. Nevertheless, the values of k_{LD}, k_{DRES}, and RR_M are to be defined based on the typical load and DRES profiles. The physical meanings of k_{LD} and k_{DRES} are that the load (or DRES) power for most of the time within a year, e.g., 99% of the time, does not vary from zero up to the nominal power but rather remains within a range equal to $(1-k_{LD})S_{tr}$ or $(1-k_{DRES})S_{tr}$. To derive the analytical expression for estimating the required BESS sizing, a 4-step method is used, which is explained in detail as follows. Note that Fig. 6 is also used to better demonstrate the basic principles of the proposed control and to facilitate the understanding of the symbols used.

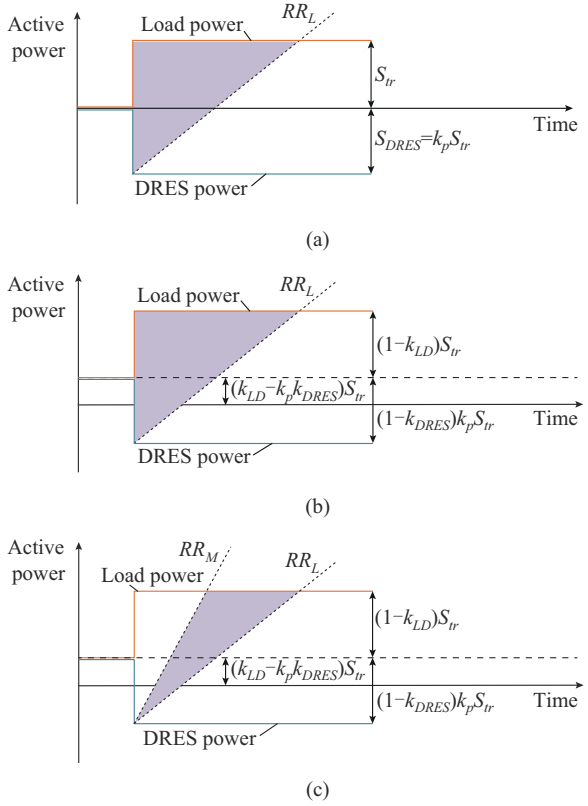

Fig. 6. BESS sizing methodology.

Step 1: the rated power of DST and the installed DRES are S_{tr} and S_{DRES}, respectively. The worst-case scenario regarding the power variation at the POI is a theoretical step change equal to $S_{tr}+S_{DRES}$, as shown in Fig. 6(a). The BESS energy in the worst-case scenario is:

$$E^{p}_{BESS} = \frac{1}{2}\frac{(S_{tr}+S_{DRES})^2}{RR_L} = \frac{1}{2}\frac{[S_{tr}(1+k_p)]^2}{RR_L} \tag{13}$$

where $S_{DRES} = k_p S_{tr}$ is a function of S_{tr}, and k_p expresses the DRES penetration in relation to the rated power of the DST ($k_p = S_{DRES}/S_{tr}$), which varies from 0 to 1. The RRL is calculated as:

$$RR_L = \frac{\Delta P}{\Delta t} = \frac{S_{tr}+S_{DRES}}{\Delta t} \tag{14}$$

Step 2: it is considered that the load within the DS does not vary from zero to the maximum installed power. *Step 2* is illustrated schematically in Fig. 6(b). Depending on the type of load or DRES, for most of the time, the active power varies between a maximum value and a minimum value, i. e., a minimum base load exists. Therefore, the load can vary in the range $[k_{LD}S_{tr}, S_{tr}]$. Similarly, the DRES power can vary in the range $[k_{DRES}S_{tr}, S_{tr}]$. Thus, the energy that the BESS needs to absorb is calculated as:

$$E^{p}_{BESS} = \frac{1}{2}\frac{\{S_{tr}[1-k_{LD}+(1-k_{DRES})k_p]\}^2}{RR_L} \tag{15}$$

Step 3: the real power variation is considered not to be in the form of a step change but rather that of a ramp with the maximum rate equal to RR_M, as shown in Fig. 6(c). For example, by analyzing several load profiles [33] that domestic loads have an RR ($\Delta P_{load}/\Delta t$) of about 50%/min-60%/min, while for industrial loads, the typical RR is 25%/min-35%/min. Thus, the total energy that the BESS stores is shown in Fig. 6 and is calculated as:

$$E^{p}_{BESS} = \frac{S^2_{tr}}{2}\left\{\frac{[1-k_{LD}+(1-k_{DRES})k_p]^2}{RR_L} - \frac{[1-k_{LD}+(1-k_{DRES})k_p]^2}{RR_M}\right\} \tag{16}$$

Step 4: finally, since the BESS must be able to absorb or release energy at any time, the total energy of the BESS is twice the energy calculated from (16) and is calculated as:

$$E_{BESS} = S^2_{tr}\left\{\frac{[1-k_{LD}+(1-k_{DRES})k_p]^2}{RR_L} - \frac{[1-k_{LD}+(1-k_{DRES})k_p]^2}{RR_M}\right\} \tag{17}$$

To calculate the maximum power that the BESS must provide to perform RR control, it is necessary to calculate the maximum power mismatch $P_{out}-P_{in}$ that might appear while P_{in} varies with RR_M and P_{out} with RR_L as:

$$P_{BESS} = S_{tr}\left(1-\frac{RR_M}{RR_L}\right)[1-k_{LD}+(1-k_{DRES})k_p] \tag{18}$$

RR_M, k_{DRES}, and k_{LD} significantly depend on the type and size of the DRES and load. Therefore, in this paper, a parametrical analysis based on real DRES and load data is presented. Table II summarizes the typical values for k_{DRES}, k_{LD}, and RR_M. These values are derived from the analysis of power profiles from loads and DRES [33]. For this purpose, the profiles from several European countries, e. g., Greece, Spain, the Netherlands, UK, Germany, and Slovenia, have been obtained, by field measurements as part of the EU Horizon 2020 project EASY-RES (G.A.: 764090).

In Table II, $k_{LD,99}$ and $k_{DRES,99}$ are the minimum values of the respective k coefficients, corresponding to the load/DRES power variation for 99% of the time within a year. Similarly, $k_{LD,95}$ and $k_{DRES,95}$ are the maximum values of the respective k coefficients, corresponding to the load/DRES power variation for 95% of the time. In the case of mixed loads (domestic and industrial) or mixed generation units (PVs and WTGs), the equivalent coefficients can be calculated from (19) - (21), using the values of Table II, where $RR_{M,\min}$ and $RR_{M,\max}$ are the minimum and maximum values of RR.

$$k_{LD} = k_{LD,dom}w_1 + k_{LD,ind}w_2 \tag{19}$$

$$k_{DRES} = k_{DRES,PV}u_1 + k_{DRES,WTG}u_2 \tag{20}$$

$$RR_M = \max\{RR_{M,dom}, RR_{M,ind}, R_{M,PV}, RR_{M,WTG}\} \tag{21}$$

TABLE II
TYPICAL VALUES FOR COEFFICIENTS PER TYPES OF LOAD AND DRES

Type of load	$k_{LD,99}$	$k_{LD,95}$	$k_{DRES,99}$	$k_{DRES,95}$	$RR_{M,\min}$ (%/min)	$RR_{M,\max}$ (%/min)
Domestic load	0.87	0.94			50	60
Industrial load	0.57	0.65			25	35
PV			0.31	0.48	30	40
WTG			0.23	0.26	55	65

VI. VALIDATION

The proposed methods are validated through simulations in MATLAB/Simulink and laboratory tests. The laboratory configuration consists of a 12-kWh 3-ph BESS from Fenecon (model: Pro 9-12), which uses lithium iron phosphate (LiFePO4) batteries. The grid is simulated using a Regenerative AC Grid Simulator (from Cinergia). Finally, an oscilloscope is used to capture the BESS voltage, current, and power. The active power reference signals of BESS are directly fed to the Pro 9-12 BESS via the Fenecon energy management system (FEMS) used to control online monitoring of BESS [34].

A. RR Control Validation

Initially, the proposed RR control is validated by means of simulations. The power at POI presents high fluctuation according to the yellow curve in Fig. 7(a). By applying the proposed RR control, RR is limited to 50 W/s. To simulate the slow response of a real BESS, a delay of 2 s is introduced into the BESS power. Figure 8 presents the validation of RR control by means of laboratory tests. Figure 8(b) depicts the reference and the actual BESS power, revealing that BESS performance in the laboratory tests is very close to the results obtained via simulation. Finally, Fig. 8(c) shows the RR with and without the proposed RR control. It is obvious that by applying the proposed RR control, RR does not exceed the limit imposed. This limit is set to be 10% of the DST rated power, i.e., ±3000 W/min.

To highlight the superiority of the proposed RR control, we compare its performance with the two most commonly used methods for RRL, i.e., LPF and MA. The most effective way to perform such a comparison is using a simple linear profile such as the one shown by Fig. 9(a). Figure 9(b) shows the calculated RR when the three methods are ap-

plied. The blue curve corresponds to P_{in} without applying any RRL. The parameters of the LPF and MA methods are selected so that in all cases, the maximum RR is not exceeded, i.e., 3000 W/min. More specifically, for LPF method, the time constant is set to be 60 s, and the rolling window of the MA is set to be 120 s. Detailed modeling of the first-order LPF and MA is presented in [14].

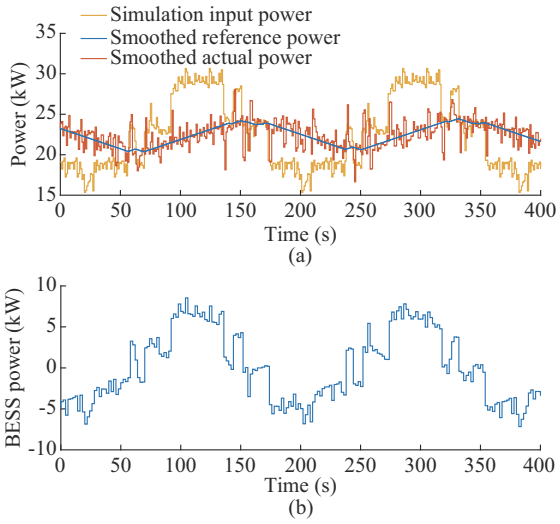

Fig. 7. Validation of RR control through simulations. (a) Simulation input power, smoothed reference power, and smoothed actual power. (b) BESS power.

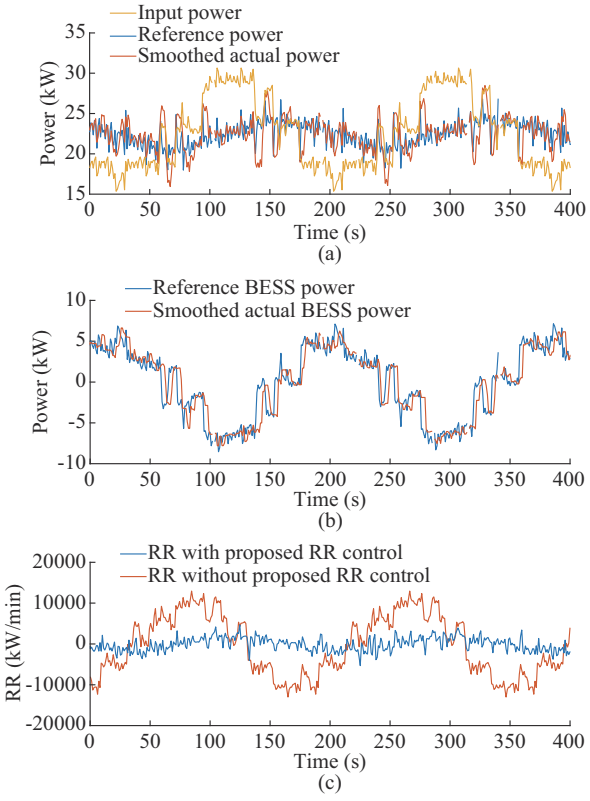

Fig. 8. Validation of RR control by means of laboratory tests. (a) Input power, reference power, and smoothed actual power. (b) Reference BESS power and smoothed actual BESS power. (c) RR with and without proposed RR control.

Through the proposed RR control, a constant RR is achieved, since RR is a control parameter. However, using the LPF or the MA method, there is a significant delay in the response because of the so-called "memory effect". The parameters of these methods cannot be directly correlated with the desired maximum RR, which leads to extensive over-smoothing and eventually to a significantly larger BESS sizing and reduced battery lifespan.

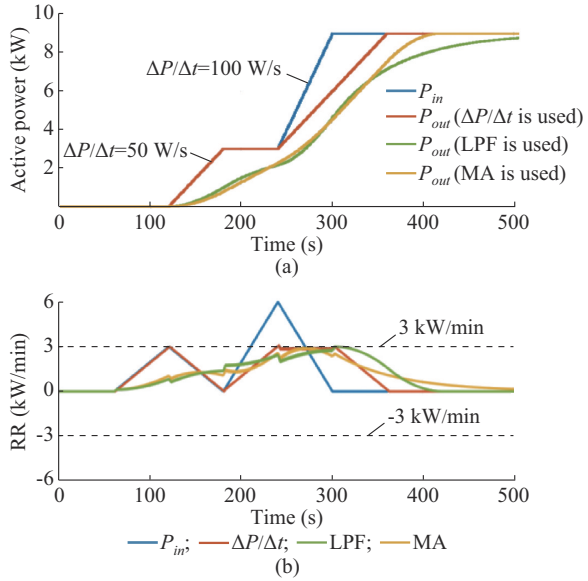

Fig. 9. Comparison of RRL methods. (a) Active power profile. (b) Calculated RR.

B. SoC Restoration Control Validation

In this subsection, the proposed control method for SoC restoration is tested. In this case, the step profile indicated by the yellow curve in Fig. 10(a) is used as the input power. The SoC restoration time is set to be 480 s, which is a typical value for BESS/RES applications [20]. The blue and red curves in Fig. 10(a) correspond to two different values of RRL that are examined: 5%/min and 10%/min of the rated DST power (30 kW). Figure 10(b) presents the BESS power for the two cases. The BESS absorbs or releases the power mismatch so that RR of the output power is maintained within the defined limit. At the same time, the proposed SoC restoration control restores SoC to the reference value of 50%, as shown in Fig. 10(c). Note that, during the SoC restoration control, the RRL is respected.

C. BESS Sizing

To evaluate the performance of the proposed method for BESS sizing, comparisons with a deterministic method are conducted. For this purpose, a detailed analytical simulation model in MATLAB/Simulink is implemented to generate power profiles at the POI (DS-TS). Further details concerning the analytical model can be found in [33]. Using the detailed simulation model, the actual BESS sizing required to limit the high-power ramps is derived. The actual BESS sizing is used as a reference point and is compared with the BESS sizing calculated by the proposed method. Different active power profiles are generated by setting the load and

DRES types and capacities as well as the respective penetration levels. Figure 11 presents the individual components that form the power exchange at the POI at a time interval of 10 days. These profiles are indicative and are obtained from field measurements [33]. Figure 11(a), (b), (c), and (d) shows the power profiles of the domestic loads, industrial loads, PVs, and WTGs, respectively.

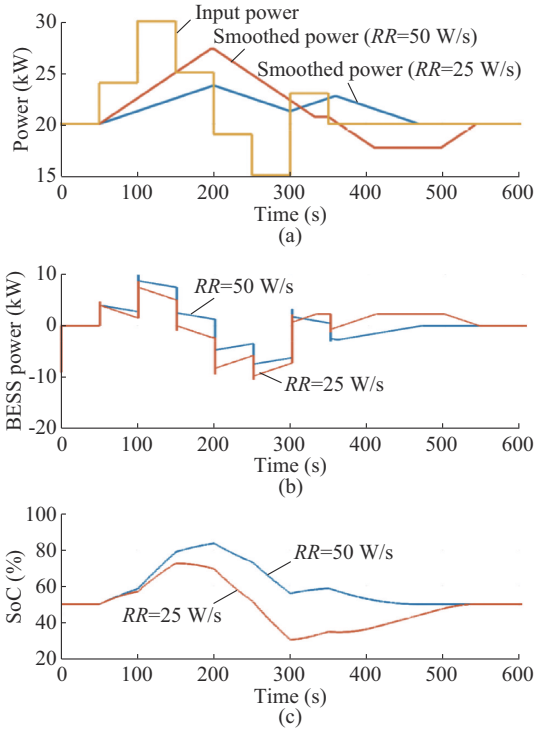

Fig. 10. Proposed SoC restoration control. (a) Input power and smoothed power. (b) BESS power. (c) SoC.

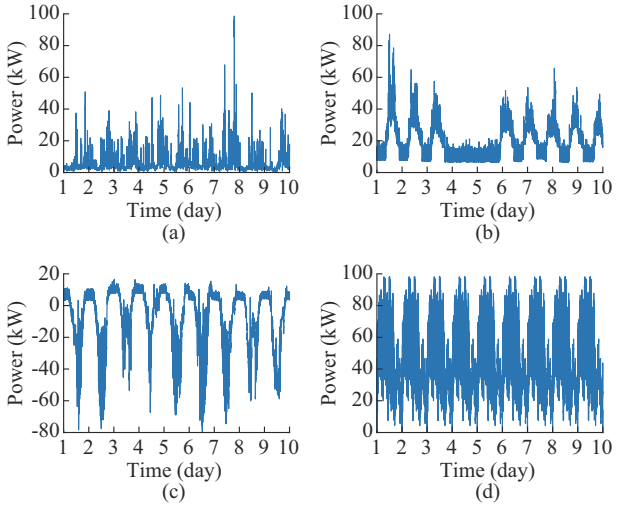

Fig. 11. Power profile. (a) Domestic load profile. (b) Industrial load profile. (c) PV power profile. (d) WTG power profile.

Based on these power profiles, the total power at the POI can be synthesized to generate different test cases. The following test cases are considered and examined.

1) Case 1: 25% DRES penetration, 100% PV, 50% domestic loads, and 50% industrial loads.

2) Case 2: 50% DRES penetration, 100% PV, 50% domestic loads, and 50% industrial loads.

3) Case 3: 75% DRES penetration, 100% PV, 50% domestic loads, and 50% industrial loads.

4) Case 4: 50% DRES penetration, 50% PV, 50% WTG, and 100% domestic loads.

Figure 12 presents the output power profile, the BESS power, and the hourly BESS energy for each examined cases obtained through the analytical model. The red dashed lines in Fig. 12(b), (d), (f), and (h) represent the estimated BESS sizing when the proposed method is used.

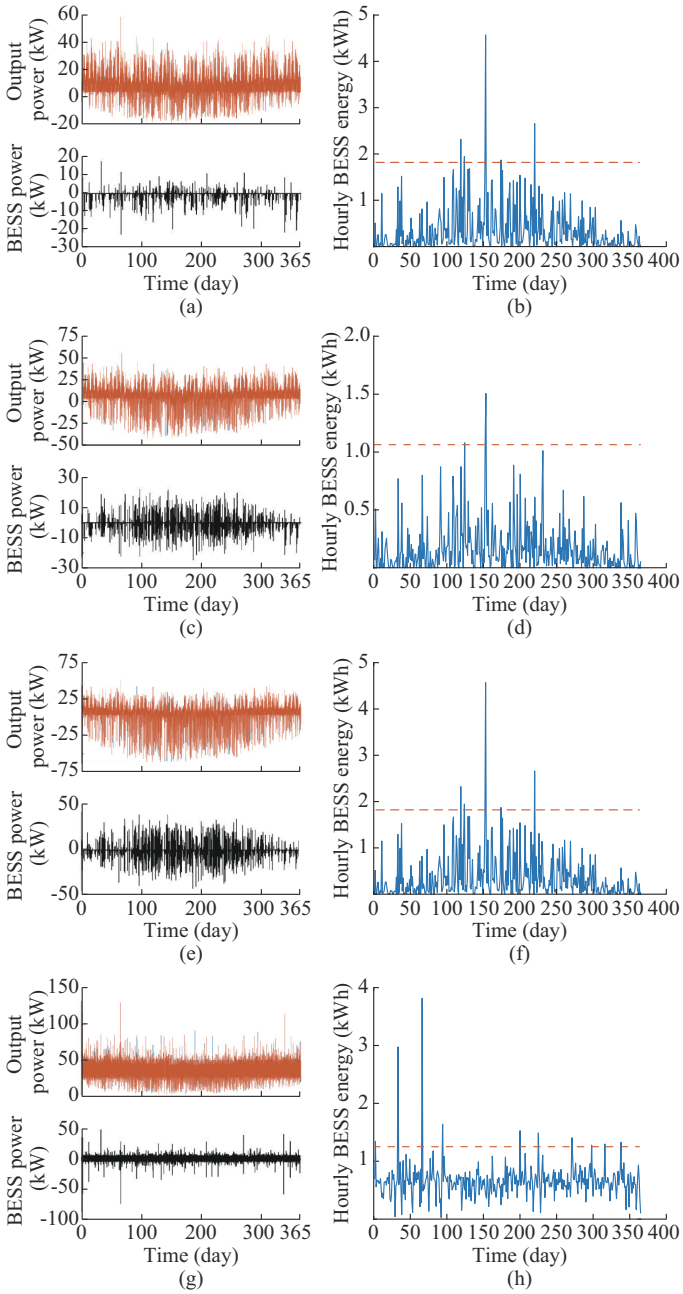

Fig. 12. Output power profile, BESS power, and hourly BESS energy for cases 1-4. (a) POI and BESS power for case 1. (b) Hourly BESS energy for case 1. (c) POI and BESS power for case 2. (d) Hourly BESS energy for case 2. (e) POI and BESS power for case 3. (f) Hourly BESS energy for case 3. (g) POI and BESS power for case 4. (h). Hourly BESS energy for case 4.

Table III presents the results for BESS capacity estimation. The analytical results with the maximum and minimum values of k_{LD} and k_{DRES} are used. Table III shows that when the maximum values are used, high-power ramps are attenuated in all examined cases by a very high percentage (>98.5%), whereas when the minimum values are used, nearly all (>99.7%) high-power ramps are limited. Note that the maximum values lead to significantly larger BESS capacity, since the worst-case scenario is considered. Based on the results, it can be concluded that using the minimum values produces good results and leads to a BESS size close to the actual size derived from the analytical MATLAB model.

TABLE III
RESULTS FOR BESS CAPACITY ESTIMATION

Case	BESS size estimation (kWh)	Smoothing percentage (%)	The maximum actual BESS size (kWh)
Case 1	The minimum: 529	99.6	785
	The maximum: 1043	100.0	
Case 2	The minimum: 1060	99.7	1929
	The maximum: 2165	100.0	
Case 3	The minimum: 1993	99.5	4623
	The maximum: 4164	99.8	
Case 4	The minimum: 1204	98.5	2372
	The maximum: 2280	99.7	

In addition to the BESS size estimation, the proposed method provides the means for estimating the BESS converter power rating. The respective results are presented in Table IV. It is proven that through the proposed method, the maximum power rating of the converter can be estimated quite precisely so that the BESS converter can provide the required power for most of the time (>99.3%) within a year.

TABLE IV
RESULTS FOR BESS POWER RATING ESTIMATION

Case	BESS power estimation (kW)	Percentage of time within a year (%)	Actual BESS power (kW)
Case 1	22.333	99.8	22.54
Case 2	25.363	100.0	24.82
Case 3	40.200	99.8	41.87
Case 4	37.116	99.3	43.48

The proposed method is proven to be accurate and be a useful tool for estimating the BESS size and the respective costs during the project design phase. The significance of the proposed method stems from the fact that the BESS size can be estimated by determining only the mixture of load and DRES. Since in this paper, RRL is considered as AS provided at the TS level and not as a system support function, the capacity estimation is rather on the safe side. The BESS size and estimated power rating can be further reduced if a simultaneity factor is used. However, this is not considered in this paper.

VII. CONCLUSION

In this paper, a holistic method is proposed for the provision of RR control as AS from DS to the upstream TS. To achieve this objective, methodologies for sizing and properly controlling a central BESS are proposed. Specifically, various definitions included in the grid codes for identifying and measuring a ramp event are presented and compared. The RR control method proposed in this paper is based on the control of $\Delta P/\Delta t$, which is adapted to the RR definition and requirements, ensuring that the actual ramp will never exceed the maximum limits imposed. In addition, the RR control is complemented with a method for restoring the SoC. The novelty of this method is that the maximum SoC restoration time can be parametrically defined, while always respecting the output power RRL. Therefore, it can be combined with the proposed control method. Furthermore, it can be adjusted to the unique characteristics of each storage technology. Finally, a novel parametric method for estimating the required BESS capacity and the power rating of the BESS converter is proposed.

The applicability of the proposed method for RRL control is validated through simulations and laboratory experiments, and comparisons with conventional methods are performed. Validation results reveal that the proposed method for RRL control can efficiently restrain RRs. The proposed method outperforms conventional methods based on LPF and MA. In addition, the proposed method for BESS sizing can correctly identify the size of the required BESS without using long-term measurements at the POI, which are difficult to obtain.

Our analysis verifies that the proposed method constitutes a holistic method that can be used to facilitate the provision of RRL as AS from DS to TS. Through the proposed method, RRL can be integrated into future AS markets as a tradable quantity.

REFERENCES

[1] G. C. Kryonidis, E. O. Kontis, T. A. Papadopoulos *et al.*, "Ancillary services in active distribution networks: a review of technological trends from operational and online analysis perspective," *Renewable and Sustainable Energy Review*, vol. 147, p. 111198, Sept. 2021.
[2] Y. Huo and G. Gruosso, "A novel ramp-rate control of grid-tied PV-battery systems to reduce required battery capacity," *Energy*, vol. 210, p. 118433, Nov. 2020.
[3] F. Blaabjerg, A. Sangwongwanich, and Y. Yang, "Chapter 6 – flexible power control of photovoltaic systems," in *Advances in Renewable Energies and Power Technologies*, Amsterdam: Elsevier, 2018, pp. 207-229.
[4] Y. Wang, N. Zhang, C. Kang *et al.*, "An efficient approach to power system uncertainty analysis with high dimensional dependencies," *IEEE Transactions on Power Systems*, vol. 33, no. 3, pp. 2984-2994, May 2018.
[5] C. S. Demoulias, K.-N. D. Malamaki, S. Gkavanoudis *et al.*, "Ancillary services offered by distributed renewable energy sources at the distribution grid level: an attempt at proper definition and quantification," *Applied Sciences–Basel*, vol. 10, no. 20, pp. 1-36, Oct. 2020.
[6] C. S. Demoulias, "Ancillary services provision in terminal distribution systems," in *Encyclopedia of Electrical and Electronic Power Engineering*, Oxford: Elsevier, 2023, pp. 411-424.
[7] Commission Regulation (EU). (2016, Apr.). Establishing a network code on requirements for grid connection of generators. [Online]. Available: https://eur-lex. europa. eu/legal-content/EN/TXT/? uri=OJ:

JOL_2016_112_R_0001
[8] ENTSO-E. (2018, Jan.). Automatic connection/reconnection and admissible rate of change of active power ENTSO-E guidance document for national implementation of conditions for automatic connection/reconnection after incidental disconnection. [Online]. Available: https://eepublicdownloads.entsoe.eu/clean-documents/Network%20codes%20documents/NC%20RfG/IGD_Conditions_for_automatic_reconnection_final.pdf
[9] G. D'Amico, F. Petroni, and S. Vergine, "Ramp rate limitation of wind power," *Energies*, vol. 15, no. 16, p. 5850, Sept. 2022.
[10] Y. Zhang, Z. Duan, and X. Liu, "Comparison of grid code requirements with wind turbine in China and Europe," in *Proceedings of 2010 Asia-Pacific Power and Energy Engineering Conference*, Chengdu, China, Mar. 2010, pp. 1-10.
[11] K.-N. Malamaki, S. I. Gkavanoudis, U. Mushtaq *et al*. (2018, Aug.). D1.1 description of the metrics developed for the quasi-steady-state operation and report on the review of the respective current grid codes. [Online]. Available: https://cordis.europa.eu/project/id/764090/results
[12] V. Gevorgian and S. Booth. (2013, May). Review of PREPA technical requirements for interconnecting wind and solar generation. [Online]. Available: https://www.nrel.gov/docs/fy14osti/57089.pdf
[13] C. Bogdan-Ionut, K. Tamas, T. Remus *et al*., "Power ramp limitation capabilities of large PV power plants with active power reserves," *IEEE Transactions on Sustainable Energy*, vol. 8, no. 2, pp. 573-581, Mar. 2017.
[14] K. N. D. Malamaki, F. Casado-Machado, M. Barragan-Villarejo *et al*., "Ramp-rate limitation of distributed renewable energy sources via supercapacitors," *IEEE Transactions on Industrial Application*, vol. 58, no. 6, pp. 7581-7594, Nov. 2022.
[15] IEEE, "Contribution to bulk system control and stability by distributed energy resources connected at distribution network," IEEE PES, New York, Tech. Rep. TR22, 2017.
[16] S. Koohi-Kamali, N. Rahim, and H. Mokhlis, "Smart power management algorithm in microgrid consisting of photovoltaic, diesel, and battery storage plants considering variations in sunlight, temperature, and load," *Energy Conversion and Management*, vol. 84, pp. 562-582, Aug. 2014.
[17] T. Kanehira, A. Takahashi, J. Imai *et al*., "A comparison of electric power smoothing control methods for distributed generation systems," *Electrical Engineering in Japan*, vol. 193, no. 4, pp. 49-57, Sept. 2015.
[18] A. Saez-de-Ibarra, E. Martinez-Laserna, and D.-I. Stroe, "Sizing study of second life Li-ion batteries for enhancing renewable energy grid integration," *IEEE Transactions on Industrial Application*, vol. 52, no. 6, pp. 4999-5008, Nov. 2016.
[19] J. Sachs, B. Müller, K. Tom *et al*., "Filter-based PV power smoothing control for island hybrid energy systems with high PV penetration," in *Proceedings of 2014 IEEE International Conference on Automation Science and Engineering*, New Taipei, China, Aug. 2014, pp. 872-877.
[20] I. de la Parra, J. Marcos, M. García *et al*., "Control strategies to use the minimum energy storage requirement for PV power ramp-rate control," *Solar Energy*, vol. 111, pp. 332-343, Jan. 2015.
[21] I. de la Parra, J. Marcos, M. García *et al*., "Storage requirements for PV power ramp-rate control in a PV fleet," *Solar Energy*, vol. 118, pp. 426-440, Aug. 2105.
[22] S. Sukumar, M. Marsadek, K. Agileswari *et al*., "Ramp-rate control smoothing methods to control output power fluctuations from solar photovoltaic (PV) sources – a review," *Journal of Energy Storage*, vol. 20, pp. 218-229, Dec. 2018.
[23] K.-N. D. Malamaki, F. Casado-Machado, M. Barragan-Villarejo *et al.*, "Ramp-rate control of DRES employing supercapacitors in distribution systems," in *Proceedings of 2021 International Conference of Smart Energy Systems and Technologies (SEST)*, virtual meeting, Dec. 2021, pp. 1-10.
[24] J. Cao, W. Du, H. Wang *et al.*, "Optimal sizing and control strategies for hybrid storage system as limited by grid frequency deviations," *IEEE Transactions on Power Systems*, vol. 33, no. 5, pp. 5486-5495, Sept. 2018.
[25] Y. Liu, W. Du, L. Xiao *et al.*, "A method for sizing energy storage system to increase wind penetration as limited by grid frequency deviations," *IEEE Transactions on Power Systems*, vol. 31, no. 1, pp. 729-737, Jan. 2016.
[26] V. T. Nguyen and J. W. Smith, "Virtual capacity of hybrid energy storage systems using adaptive state of charge range control for smoothing renewable intermittency," *IEEE Access*, vol. 8, pp. 126951-126964, Jan. 2020.
[27] K. Lappalainen and S. Valkealahti, "Sizing of energy storage systems for ramp rate control of photovoltaic strings," *Renewable Energy*, vol. 196, pp. 1366-1375, Aug. 2022.
[28] D. Alvaro, R. Arranz, and J. A. Aguado, "Sizing and operation of hybrid energy storage systems to perform ramp-rate control in PV power plants," *International Journal of Electrical Power & Energy Systems*, vol. 107, pp. 589-596, May 2019.
[29] Y. Yang, S. Bremner, C. Menictas *et al*., "Battery energy storage system size determination in renewable energy systems: a review," *Renewable and Sustainable Energy Reviews*, vol. 91, pp. 109-125, Aug. 2018.
[30] H. Tahir, D.-H. Park, S.-S. Park *et al*., "Optimal ESS size calculation for ramp rate control of grid-connected microgrid based on the selection of accurate representative days," *International Journal of Electrical Power & Energy Systems*, vol. 139, p. 108000, Jul. 2022.
[31] A. Abbassi, M. A. Dami, and M. Jemli, "A statistical approach for hybrid energy storage system sizing based on capacity distributions in an autonomous PV/wind power generation system," *Renewable Energy*, vol. 103, pp. 1-10, Apr. 2017.
[32] M. Huber, D. Dimkova, and T. Hamacher, "Integration of wind and solar power in Europe: assessment of flexibility requirements," *Energy*, vol. 69, pp. 236-246, May 2014.
[33] K.-N. Malamaki, S. I. Gkavanoudis, S. Giazitzis *et al*. (2021, Jul.). D1.7 Final report (after feedback form lab tests) presenting: the reactive power control algorithm for converter-interfaced DRES/BESS, the analytical tool for parametric BESS sizing for low-frequency power smoothing and the analytical tool for the evaluation of the converter operational losses due to exchange of reactive power. [Online]. Available: https://cordis.europa.eu/project/id/764090/results
[34] A. Shekhar, S. Venu, K.-N. Malamaki *et al*. (2021, Jul.). D6.2 report on the laboratory tests. [Online]. Available: https://cordis. europa. eu/project/id/764090/results

Spyros I. Gkavanoudis received the Diploma and Ph.D. degrees in electrical and computer engineering from the Department of Electrical and Computer Engineering at Aristotle University of Thessaloniki (AUTH), Thessaloniki, Greece, in 2008 and 2014, respectively. Currently, he is a Post-Doctoral Researcher at the same University and works for the Greek DSO (HEDNO). From 2009 till 2022, he was an Adjunct Lecturer at the Department of Electrical and Computer Engineering at the AUTH and University of Thessaly, Thessaly, Greece. He has a 6-year experience as a Researcher in EU (H2020) projects. His research interests include power electronic converters, wind energy conversion systems, modeling and control of electrical machines, energy storage systems and protection of distribution grids.

Kyriaki-Nefeli D. Malamaki received the Dipl. and Ph.D. degrees in electrical and computer engineering from the Department of Electrical and Computer Engineering (DECE) at Aristotle University of Thessaloniki (AUTH), Thessaloniki, Greece, in 2012 and 2020, respectively. Currently, she is a Post-doctoral Researcher at the DECE, AUTH and works as a Freelance Researcher in European-funded projects for the Greek TSO, Independent Power Transmission Operator. From 2021 till 2022, she was an Adjunct Lecturer at the DECE, AUTH. She has a 6-year experience as a Researcher in EU (H2020) and national research projects. Her research interests include distributed generation and storage, power quality, interface of renewable energy sources with the grid, power electronic converters control and energy storage systems integration within the smart grid context.

Eleftherios O. Kontis received the Dipl. (Eng.) and Ph.D. degrees in electrical engineering from the Department of Electrical and Computer Engineering, Aristotle University of Thessaloniki (AUTH), Thessaloniki, Greece, in 2013 and 2018, respectively. He is currently a Research Associate with the AUTH and an Adjunct Lecturer with the Department of Industrial Engineering and Management at International Hellenic University, Thessaloniki, Greece. He also works as a Power System Engineer with the Southeast Electricity Network Coordination Center. His research interests include power system modeling and dynamic analysis, distributed generation, operation and control of active distribution networks, and real-time analysis of power systems through field measurements.

Aditya Shekhar received the bachelor's degree in electrical from the National Institute of Technology, Surat, India, in 2010, and the M.Sc. (cum laude) and Ph.D. degrees in electrical engineering from the Delft University of Technology, Delft, The Netherlands, in 2015 and 2020, respectively. He is currently an Assistant Professor with the Delft University of Technology. His research interests include reliable power electronic systems for enabling energy transition.

Umer Mushtaq received the B.Sc. degree in electrical and electronic engineering from the University of Engineering and Technology Lahore, Lahore, Paki-

stan. He received the master's degree in Sustainable Transportation and Electrical Power Systems from the University of Oviedo, Oviedo, Spain. He is now a Ph.D. candidate at Delft University of Technology, Delft, The Netherlands. He worked three years at Fatima Group LTD as a Project and Design Engineer. In 2013, he was awarded an Erasmus Mundus joint master's degree Scholarship from Education, Audiovisual and Culture Executive Agency of the European Union. His research interests include hybrid reactive power compensation system (Hybrid-STATCOM) for low voltage applications with OPAL RT hardware in the loop system.

Sagar Bandi Venu received the B.E degree in computer science from Visvesvaraya Technological University in Bangalore, Bangalore, India, in 2013, and the M.Sc. degree in The University of Passau, Passau, Germany, in 2019. He works for FENECON GmbH, Deggendorf, Germany, as a Software Developer in the Energy Management System Department. His main area of expertise is designing and developing energy management controllers, which he implements in OpenEMS, an open-source platform for energy management applications.

Charis S. Demoulias received the Dipl. and Ph.D. degrees in electrical engineering from the Aristotle University of Thessaloniki (AUTH), Thessaloniki, Greece, in 1984 and 1991, respectively. Currently, he is Professor with the Electrical Machines Laboratory, Department of Electrical and Computer Engineering, AUTH. From 1991 to 2003, he co-founded Alteren SA, a technical consulting company offering consultancy services in private and public energy-saving and renewable energy projects and he also acted as Contractor for power quality projects (harmonic filters), industrial energy-saving projects and photovoltaic installations (stand-alone and grid-connected). He has participated as Coordinator or Partner in seven EU-funded projects and six national projects. His research interests include power electronics, harmonics, electric motion systems, and the integration of renewable energy sources in the power grid.